AD-A104 242 HARVARD UNIV CAMBRIDGE MA GORDON MCKAY LAB F/G 20/14
SCATTERING OF ELECTROMAGNETIC WAVES BY OBSTACLES IN THE PRESENC--ETC(U)
AUG 81 H LEE, T T WU, R W KING DAAG29-79-C-0109
UNCLASSIFIED ARO-16297.1-EL NL

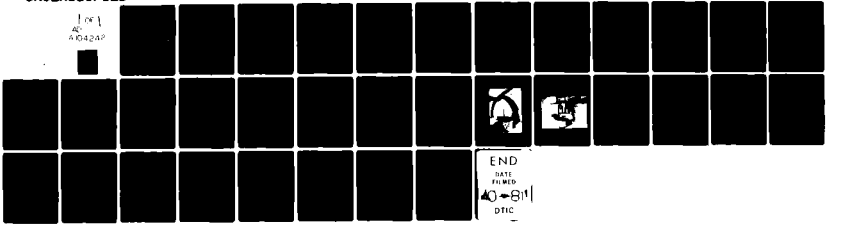

(12) LEVEL II

SCATTERING OF ELECTROMAGNETIC WAVES BY OBSTACLES IN THE PRESENCE OF THE EARTH'S SURFACE.

FINAL REPORT

Hung-Mou Lee, Tsun Wu, Ronold W. P. King

Aug 1981

U. S. Army Research Office
Contract Number DAAG29-79-C-0109

Gordon McKay Laboratory
Harvard University
Cambridge, Massachusetts 02138

Approved for public release; distribution unlimited.

THE FINDINGS IN THIS REPORT ARE NOT TO BE CONSTRUED AS AN OFFICIAL DEPARTMENT OF THE ARMY POSITION, UNLESS SO DESIGNATED BY OTHER AUTHORIZED DOCUMENTS.

UNCLASSIFIED

SECURITY CLASSIFICATION OF THIS PAGE (When Data Entered)

REPORT DOCUMENTATION PAGE	READ INSTRUCTIONS BEFORE COMPLETING FORM
1. REPORT NUMBER	2. GOVT ACCESSION NO. AD-A104 242	3. RECIPIENT'S CATALOG NUMBER
4. TITLE (and Subtitle) SCATTERING OF ELECTROMAGNETIC WAVES BY OBSTACLES IN THE PRESENCE OF THE EARTH'S SURFACE	5. TYPE OF REPORT & PERIOD COVERED Final Report 7/1/79 - 6/30/81
	6. PERFORMING ORG. REPORT NUMBER
7. AUTHOR(s) H. M. Lee, T. T. Wu, and R. W. P. King	8. CONTRACT OR GRANT NUMBER(s) DAAG29-79-C-0109
9. PERFORMING ORGANIZATION NAME AND ADDRESS Gordon McKay Laboratory Harvard University Cambridge, MA 02138	10. PROGRAM ELEMENT, PROJECT, TASK AREA & WORK UNIT NUMBERS DRXRO-PR P-16297-EL
11. CONTROLLING OFFICE NAME AND ADDRESS U.S. Army Research Office P.O. Box 12211 Research Triangle Park, NC 27709	12. REPORT DATE August 31, 1981
	13. NUMBER OF PAGES 26
14. MONITORING AGENCY NAME & ADDRESS(if different from Controlling Office)	15. SECURITY CLASS. (of this report) UNCLASSIFIED
	15a. DECLASSIFICATION/DOWNGRADING SCHEDULE

16. DISTRIBUTION STATEMENT (of this Report)

Approved for public release; distribution unlimited.

17. DISTRIBUTION STATEMENT (of the abstract entered in Block 20, if different from Report)

18. SUPPLEMENTARY NOTES

19. KEY WORDS (Continue on reverse side if necessary and identify by block number)

Fat tubular cylinder
Effect of dissipative half-space
Scattered field
Theory and experiment

20. ABSTRACT (Continue on reverse side if necessary and identify by block number)

The electromagnetic scattering from a geometrically fat tubular cylinder above a dissipative dielectric half-space has been investigated. Extensive experimental data were obtained and were found to be in agreement with theoretical results. The theory made use of an explicit analytical solution of the scattering from such a cylinder when in a single medium. Because the cylinder is a finite object with two variable geometrical parameters, it represents a very useful model for future experimental studies on the scattering from more complicated objects.

DD FORM 1 JAN 73 1473 EDITION OF 1 NOV 65 IS OBSOLETE

UNCLASSIFIED

SECURITY CLASSIFICATION OF THIS PAGE (When Data Entered)

TABLE OF CONTENTS

LIST OF ILLUSTRATIONS

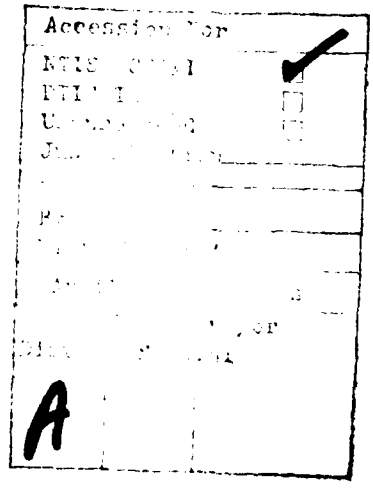

TABLE HEADING

SUMMARY

The purpose of this research project has been to study the electromagnetic scattering from conducting objects on or near the surface of the earth. A theoretical analysis of the scattering from real targets such as vehicles on the earth or low-flying airplanes or cruise missiles has not been possible. Hence, efforts have been concentrated on extensive experimental measurements of theoretically manageable, simpler structures which can be used later to simulate real targets.

Although linear dipoles, crossed dipoles, and wire loops have been used as scattering obstacles in free space or above the earth, the present investigation has been concerned primarily with the scattering from a set of geometrically fat tubular cylinders. This choice was made not only because an exact, free-space solution for the scattering from such a tubular cylinder was obtained during the course of this study, but also because this structure represents a 'composite' object which consists of a stack of wire loops. Thus, the scattering characteristics of a real target on or above the earth can be compared with those of fat cylinders of varying heights and diameters by means of a theoretical algorithm which made use of our knowledge of the free-space solution and has been proved accurate by experimental check.

It is important to note that, although one can physically stack-up straight wires or wire loops to form a surface, to extend the well-known theoretical results for the scattering from a straight wire or a wire loop to a stack of straight wires or wire loops is a forbidding task. These well-known solutions are essentially the lowest-order approximate solutions in terms of the wire radius. Two difficulties would arise if straight wires or wire loops were used as models of finite objects on or near the earth's surface. First, meshes could be formed out of the wires. The linear solutions could be applied directly but, as the spacing of the meshes was reduced, the radius of the wires could not be ignored and a higher-order solution would be required. The second problem would occur if a wire were moved close to the earth's surface. The decrease in distance between the wire and the earth would again render the lowest-order approximation inadequate. Even the important paper by King, Wu and Shen [1] did not address this problem.*

*The infinite horizontal wire treated in this paper could not be laid on the

The exact solution for the scattering current on a fat tubular cylinder in free space removed all of these problems. Since no approximation was involved in its dimensions, the fat tubular cylinder could be located on the earth's surface or hung vertically in the air. An algorithm was implemented which gives the solution for the scattering current of a fat tubular cylinder in the presence of a (dissipative) dielectric half-space. The computed bistatic scattered fields appear to be in agreement with an extensive list of experimentally measured data of the scattered fields from eighteen different tubular cylinders at twenty-three different heights above water.

---

ground. It was conceived that the trouble was caused by the particular formulation of the problem rather than by the analysis involved.

1. THE EXPERIMENT

1.1. Mechanical Setup

This experiment was carried out indoors. Due to space limitations and equipment availability, the wavelength of 20 cm was chosen. At this frequency and with a temperature of 22.5 ± 1 °C when the data were taken, the complex dielectric constant of the water was estimated to be 78(1.0 + i.09). An octagonal water tank was constructed. With diagonals of 3.40 meters and a depth of roughly 60 cm, it was used to simulate an infinite half-space of water. A semicircular styrofoam arch was erected over the tank to hold the transmitting and receiving antennas. The inner and outer radii of the semicircular arch were 2.0 meters and 2.3 meters, respectively. The whole system was partially enclosed by microwave absorbers. Pictures showing the setup from different viewing angles are in Figs. 1 and 2. Hung from the highest part of the semicircular arch to its center by four pieces of mono-filament nylon line was a 5-cm thick styrofoam block with a 50 × 50 cm^2 surface. A disc of about 40 cm in diameter was removed from the center of the block. Eighteen identical discs were constructed, each with a fat tubular cylinder embedded in the lower side so that the cylinders could be placed very close to the water surface. Schematic diagrams of the mechanical setup and the associated coordinate system appear in Figs. 3 and 4; a diagram of the cross section of one of the styrofoam discs and its holder appears in Fig. 5.

1.2. Measuring Techniques

Because a continuous-wave generator was used, a constant background radiation was present with an intensity much stronger than the signal scattered from the tubular cylinders. Figure 6 shows the block diagram that incorporates a cancellation circuit. From the -30 dB monitor of the microwave generator, a current was led through a variable attenuator and a line stretcher to a hybrid, where it was combined with the field picked up by the receiving antenna. An empty styrofoam disc was put into the holder as a reference. The variable attenuator and the line stretcher in the cancellation circuit were adjusted so that the combined signal produced a null reading on the vector voltmeter. The empty styrofoam disc was then replaced by one containing a fat tubular cylinder. The resulting amplitude and phase reading was the desired signal.

The transmitting and receiving antennas, which were 6-element Yagi-Uda

arrays, were located at 45° angles from the normal on opposite sides of the styrofoam arch with their polarizations parallel to the surface of the water. The distance between the driving element of each antenna array to the center of the fat tubular cylinder was measured to be 249.84 cm. The incident and receiving angles of the polarizations of the antennas could be changed, but they remained fixed in the present experiment.

Attention was directed to the determination of the dependence of the scattered field on the size of the fat tubular cylinder and on its height above the water. The radii of the eighteen fat tubular cylinders varied from 11 cm to 36 cm in circumference. The width of the fat tubular cylinders was fixed at 0.5 cm. The height of the fat tubular cylinder above the water, which was changed by lowering or raising the water level in the tank, varied from less than 1 cm to 20 cm.

The scattered signal was measured against a reference field proportional to the power going into the transmitting antenna. The reference signal was about 6 mW, while the power going to the antenna was close to 60 W.

1.3. Experimental Data

In terms of the coordinate system shown in Fig. 4, the y-component of the field scattered from eighteen different fat tubular cylinders was measured. The fat tubular cylinders had a fixed width (0.5 cm) and varying radius b with $k_1 b$ = 0.550, 0.625, 0.700, 0.775, 0.850, 0.925, 1.000, 1.075, 1.150, 1.225, 1.300, 1.375, 1.450, 1.500, 1.575, 1.650, 1.725, 1.800. The height h of the center of the fat tubular cylinder above the water surface was increased in 24 steps so that $2h/\lambda$ = 0.085, 0.135, 0.185, 0.235, 0.285, 0.335, 0.385, 0.435, 0.485, 0.535, 0.585, 0.635, 0.685, 0.785. 0.885, 0.985, 1.085, 1.185, 1.285, 1.385, 1.485, 1.585, 1.785, 1.985. Note that $k_1 = 2\pi/\lambda$ and λ = 20 cm. Measurements of the fields scattered from all of the eighteen fat tubular cylinders were made at one height before the water level in the tank was lowered, thus effectively raising the height of the disc holder to the next height. Since only the water level was changed, the reference signal to the vector voltmeter was always proportional to that portion of the electric field at the center of the fat tubular cylinder which was radiated directly from the transmitting antenna, referred to as the 'direct incident field.' Since the elements of the receiving antenna array were pointing in the y-direction, the signal reading on the vector volt-

meter after the background radiation was subtracted out was proportional to the y-component of the scattered electric field (this included the scattered field reflected by the water) at the receiving antenna due to the surface current distribution on the fat tubular cylinder.

The measured results are listed in Table 1 as a ratio of the direct voltage readings on the vector voltmeter of the received signal V^{sc} to a reference signal V_r. The reference signal came from a directional coupler which picked up a -20 dB signal from the wave that traveled in the direction from the power generator to the transmitting antenna in the transmission line connecting these two points. Accompanying these magnitude and phase values is a (complex) constant multiple of V^{sc}/V_r, denoted by E^{sc}/E_0, which is the ratio of the scattered field at the location of the receiving antenna to the direct incident field at the center of the fat tubular cylinder. Note that because both the transmitting and receiving antennas have their conducting elements parallel to the y-axis, E^{sc} is the y-component of the scattered electric field while E_0 has only a y-component. The constant factor was derived by comparing measured data with theoretically computed results; the E^{sc}/E_0 values are plotted against theoretical curves in Figs. 7 through 24.

1.4. Comparison of Theoretical Results with Experimental Data

A numerical solution for the surface current distribution was programmed in FORTRAN IV and executed on the VAX-11/780 computer located at the Dunbar Lab., Harvard University. The y-component of the scattered field, E^{sc}, at the receiving antenna was evaluated so that a comparison with experimental results could be made. Incident fields in the form of either a plane wave or a field radiated by a point dipole source located at the position of the transmitting antenna were used. In either case, the direct incident field was normalized so that at the center of the fat tubular cylinder E_0 equals 1 and is pointing in the positive y-direction. Thus, the computed scattered field equals E^{sc}/E_0. The agreement with experimental data turned out to be better when the incident field originated from a dipole source, although the difference was not significant.

Theoretical curves of E^{sc}/E_0 for different fat tubular cylinders are plotted in Figs. 7 through 24 as functions of $2h/\lambda$. Note that the phases have been plotted in units of π.

The ratio $(E^{sc}/E_0)/(V^{sc}/V_r)$ should be constant, as pointed out in Section

1.1. Average values were taken separately of the magnitudes and phases of $(E^{sc}/E_0)/(V^{sc}/V_r)$ for all experimental data, with those deviating from the average by more than 20% excluded. The resulting normalization constant has a magnitude of 0.0330 and a phase of -0.558π. Experimental values of E^{sc}/E_0, obtained by multiplying V^{sc}/V_r by this normalization constant, are also listed in Table 1 and are plotted against the theoretical curves in Figs. 7 through 24. The agreement is good.

1.5. Remarks and Conclusion

Very extensive experimentally measured results have been obtained. The data appear to confirm the validity of the theoretical algorithm used in computing the scattering current. In the range $2h/\lambda < 1.4$, Figs. 7 through 13 show that the strongest signals appear at about $2h/\lambda = 0.7$. Thus, the location of the peak for k_1b less than 1.0 follows the strength of the total incident field, which includes the direct incident field radiated by the transmitting antenna and the reflection from the water. The magnitude of the peak depends on the size of the fat tubular cylinder and falls between $k_1b = 1.000$ and 1.075 in Figs. 13 and 14, as one would expect from free-space scattering from fat tubular cylinders. The peak of the magnitude of the scattered field shifts toward larger $2h/\lambda$ values until a maximum of the magnitude is reached at $k_1b = 1.150$ and $2h/\lambda = 0.91$ in Fig. 15. This indicates that there is a resonance due to the interaction between the cylinder and the water. The magnitude of the scattered field for $k_1b = 1.150$ in Fig. 15 falls below the curves for $k_1b = 1.000$ and $k_1b = 1.075$ for $2h/\lambda$ less than 0.4 in Figs. 13 and 14. This fact shows that the resonance is not related to the free-space resonances of the fat tubular cylinders. For larger cylinders, the location $(2h/\lambda)$ of the peak decreases with increasing cylinder sizes until it returns to near 0.7 when $k_1b = 1.725$ in Fig. 23.

It would be rewarding to compare the resonance characteristics of the vertical fat tubular cylinder to those of a horizontal cylinder of properly chosen dimensions above the water because the $n = 1$ Fourier component of the fat tubular cylinder contributes most strongly to the scattered field. Any similarity between these two cases would be helpful in generalizing the results for the fat tubular cylinder case to other more complicated real targets.

2. THE THEORY

2.1. Scattering from a Geometrically Fat Tubular Cylinder in Free Space

A perfectly conducting tubular cylinder can be described by two geometrical parameters, namely, its height and its radius. It is 'thin' or 'fat' depending on whether its height is larger than its radius or vice versa. In the presence of a time-harmonic sinusoidal electromagnetic field, these parameters are measured against the wavelength. The distribution of surface current appears on the tubular cylinder and oscillates with the external field except for the restriction that it has to lie within the boundaries of the tubular cylinder. The theory is devoted to the detailed surface current distribution which is excited by the external field but is dictated by the particular geometry of the tubular cylinder. Hence, the high-frequency, geometrical-optics aspect of the problem, in which the geometrical restriction of the object is only marginal, is excluded implicitly. Thus, at least one of the two parameters of the tubular cylinder under consideration is not much larger than the wavelength.

The distinction between a 'fat' or a 'thin' tubular cylinder is important under these circumstances. The two geometrical parameters give the bounds in each direction within which the surface current must exist. The implication is that the smaller parameter determines the basic size of geometrical building blocks, called 'patches,' in which the surface current varies with the same magnitude in both directions. (This fact is meaningless in geometrical optics because only the wavelength is the determining factor in that limit.) As shown in Fig. 25, on a fat tubular cylinder a 'patch' is a bended rectangular strip covering a square area; on a thin tubular cylinder a 'patch' is a tubular cylinder which has its height equal to its diameter. The picture of the patches on a tubular cylinder provides an interpolation from the two limiting cases of a tubular cylindrical structure, viz., a thin-wire loop and a thin straight wire. In fact, the power-series expansion of e^{ikR}/R in squares of the height of a fat tubular cylinder has been interpreted [2] as a series expansion of the interaction among patches in terms of the interaction strength of the current distribution within a patch. Such a power-series expansion has led to an iterative scheme which calls for the use of Tchebichef polynomials to represent the surface current distribution and gives, to all orders, the explicit forms of the scattering current on a fat tubular cylinder.

2.2. Scattering from a Fat Tubular Cylinder above a Dissipative Dielectric Half-Space

Tchebichef polynomials have been used, as in the free-space case, to represent the surface current distribution on the fat tubular cylinder when it is hung above the water. Numerical integration was used to compute the parts of the kernel involving Sommerfeld-type integrals. The results were compared with the extensive experimental data obtained earlier and found to be in agreement [2].

3. CONCLUSION

The fat tubular cylinder has been studied extensively. The algorithm devised to obtain the scattering surface current distribution on such a cylinder has proved to be useful. Furthermore, because orthonormal polynomials were used in the theoretical treatment of this problem, higher-order solutions could be generated without having to redo any of the numerical integration already carried out.

With the two geometrical parameters which could be varied independently, and with the availability of the theoretical solutions, the fat tubular cylinder has become an ideal model for use in future experimental studies of more complicated objects.

REFERENCES

[1] R. W. P. King, T. T. Wu, and L. C. Shen, "The horizontal-wire antenna over a conducting or dielectric half-space: Current and admittance," Radio Sci., vol. 9, pp. 701-709, July 1974.

[2] H. M. Lee, "Electromagnetic scattering of a loop above a half-space: Theory and experiment," Ph.D. Thesis, Harvard University, Cambridge, MA, 1981.

$2h/\lambda$	$k_1 b$	V^{sc}/V_r		E^{sc}/E_0	
		Magnitude	Phase (π)	Magnitude	Phase (π)
0.085	0.925	0.073	-0.844	0.0022	-1.402
	1.000	0.093	-0.638	0.0028	-1.196
	1.075	0.083	-0.433	0.0025	-0.991
	1.150	0.081	-0.369	0.0024	-0.927
0.135	0.925	0.133	-0.933	0.0040	-1.491
	1.000	0.269	-0.661	0.0082	-1.219
	1.075	0.224	-0.400	0.0068	-0.958
	1.150	0.177	-0.317	0.0054	-0.875
0.185	0.925	0.204	-0.889	0.0062	-1.447
	1.000	0.315	-0.611	0.0096	-1.169
	1.075	0.340	-0.361	0.0103	-0.919
	1.150	0.270	-0.278	0.0082	-0.836
	1.225	0.269	------	0.0082	------
	1.375	0.217	------	0.0066	------
	1.500	0.173	------	0.0053	------
	1.650	0.124	------	0.0038	------
	1.800	0.160	------	0.0049	------
0.235	0.925	0.294	-0.822	0.0089	-1.380
	1.000	0.481	-0.561	0.0146	-1.119
	1.075	0.447	-0.322	0.0135	-0.880
	1.150	0.364	-0.258	0.0110	-0.816
0.285	0.925	0.528	-0.733	0.0160	-1.291
	1.000	0.813	-0.500	0.0246	-1.058
	1.075	0.750	-0.303	0.0227	-0.861
	1.150	0.634	-0.217	0.0192	-0.775
0.335	0.925	0.624	-0.661	0.0189	-1.219
	1.000	0.908	-0.463	0.0275	-1.021
	1.075	0.888	-0.286	0.0269	-0.844
	1.150	0.774	-0.194	0.0234	-0.752
0.385	0.925	0.712	-0.581	0.0216	-1.139
	1.000	0.960	-0.406	0.0291	-0.964
	1.075	0.982	-0.239	0.0297	-0.797
	1.150	0.900	-0.150	0.0273	-0.708
0.435	0.925	0.762	-0.519	0.0231	-1.077
	1.000	1.010	-0.361	0.0306	-0.919
	1.075	1.078	-0.217	0.0327	-0.775
	1.150	1.018	-0.125	0.0309	-0.683

Table 1 Measured Scattered Fields

$2h/\lambda$	$k_1 b$	V^{sc}/V_r		E^{sc}/E_0	
		Magnitude	Phase (π)	Magnitude	Phase (π)
0.485	0.925	0.776	-0.447	0.0235	-1.005
	1.000	1.063	-0.300	0.0322	-0.858
	1.075	1.205	-0.169	0.0365	-0.727
	1.150	1.139	-0.078	0.0345	-0.636
0.535	0.925	0.797	-0.381	0.0241	-0.939
	1.000	1.069	-0.256	0.0324	-0.814
	1.075	1.256	-0.117	0.0381	-0.675
	1.150	1.249	-0.019	0.0379	-0.577
	1.225	1.196	0.031	0.0362	-0.527
	1.300	1.070	0.058	0.0324	-0.500
0.585	0.925	0.805	-0.299	0.0244	-0.857
	1.000	1.073	-0.177	0.0325	-0.735
	1.075	1.293	-0.046	0.0392	-0.604
	1.150	1.319	0.040	0.0400	-0.518
	1.225	1.295	0.095	0.0392	-0.463
	1.300	1.178	0.140	0.0357	-0.418
	1.375	1.075	0.198	0.0326	-0.360
	1.450	0.958	0.206	0.0290	-0.352
	1.500	0.891	0.204	0.0270	-0.354
	1.575	0.790	0.199	0.0239	-0.359
	1.650	0.725	0.116	0.0220	-0.442
	1.725	0.769	0.035	0.0233	-0.523
	1.800	1.053	-0.068	0.0319	-0.626
0.635	0.550	0.127	-0.522	0.0038	-1.080
	0.625	0.207	-0.506	0.0063	-1.064
	0.700	0.323	-0.494	0.0098	-1.052
	0.775	0.483	-0.433	0.0146	-0.991
	0.850	0.695	-0.347	0.0211	-0.905
	0.925	0.950	-0.225	0.0288	-0.783
	1.000	1.255	-0.144	0.0380	-0.702
	1.075	1.504	-0.005	0.0456	-0.563
	1.150	1.579	0.090	0.0478	-0.468
	1.225	1.477	0.151	0.0448	-0.407
	1.300	1.365	0.195	0.0414	-0.363
	1.375	1.213	0.220	0.0368	-0.338
	1.450	1.082	0.234	0.0328	-0.324
	1.500	0.992	0.231	0.0300	-0.327
	1.575	0.871	0.223	0.0264	-0.335
	1.650	0.788	0.181	0.0239	-0.377
	1.725	0.824	0.091	0.0250	-0.467
	1.800	1.117	0.003	0.0338	-0.555

Table 1 (continued)

$2h/\lambda$	$k_1 b$	V^{sc}/V_r		E^{sc}/E_0	
		Magnitude	Phase (π)	Magnitude	Phase (π)
0.685	0.850	0.687	-0.283	0.0208	-0.841
	0.925	0.950	-0.189	0.0288	-0.747
	1.000	1.279	-0.083	0.0387	-0.641
	1.075	1.547	0.042	0.0469	-0.516
	1.150	1.625	0.144	0.0492	-0.414
	1.225	1.583	0.206	0.0480	-0.352
	1.300	1.430	0.250	0.0433	-0.308
	1.375	1.291	0.267	0.0391	-0.291
	1.450	1.142	0.284	0.0346	-0.274
	1.500	1.054	0.287	0.0319	-0.271
	1.575	0.935	0.264	0.0283	-0.294
	1.650	0.837	0.217	0.0254	-0.341
	1.725	0.851	0.137	0.0258	-0.421
	1.800	1.106	0.051	0.0335	-0.507
0.785	0.925	0.849	-0.086	0.0257	-0.644
	1.000	1.171	0.011	0.0355	-0.547
	1.075	1.504	0.128	0.0456	-0.430
	1.150	1.671	0.233	0.0506	-0.325
	1.225	1.631	0.306	0.0494	-0.252
	1.300	1.484	0.364	0.0450	-0.194
	1.375	1.320	0.392	0.0400	-0.166
	1.450	1.174	0.417	0.0356	-0.141
	1.500	1.087	0.422	0.0329	-0.136
	1.575	0.951	0.417	0.0288	-0.141
	1.650	0.843	0.372	0.0256	-0.186
	1.725	0.787	0.306	0.0239	-0.252
	1.800	0.941	0.211	0.0285	-0.347
0.885	0.925	0.810	-0.003	0.0245	-0.561
	1.000	1.142	0.089	0.0346	-0.469
	1.075	1.559	0.208	0.0472	-0.350
	1.150	1.917	0.322	0.0581	-0.236
	1.225	1.846	0.408	0.0559	-0.150
	1.300	1.598	0.478	0.0484	-0.080
	1.375	1.332	0.519	0.0404	-0.039
	1.450	1.153	0.539	0.0349	-0.019
	1.500	1.014	0.552	0.0307	-0.006
	1.575	0.872	0.552	0.0264	-0.006
	1.650	0.723	0.513	0.0219	-0.045
	1.725	0.637	0.462	0.0193	-0.096
	1.800	0.726	0.357	0.0220	-0.201

Table 1 (continued)

$2h/\lambda$	$k_1 b$	V^{sc}/V_r		E^{sc}/E_0	
		Magnitude	Phase (π)	Magnitude	Phase (π)
0.985	0.550	0.085	-0.133	0.0026	-0.691
	0.625	0.127	-0.094	0.0038	-0.652
	0.700	0.184	-0.061	0.0056	-0.619
	0.775	0.271	-0.011	0.0082	-0.569
	0.850	0.390	0.031	0.0118	-0.527
	0.925	0.643	0.089	0.0195	-0.469
	1.000	0.947	0.172	0.0287	-0.386
	1.075	1.461	0.292	0.0443	-0.266
	1.150	1.671	0.442	0.0506	-0.116
	1.225	1.535	0.550	0.0465	-0.008
	1.300	1.281	0.625	0.0388	0.067
	1.375	1.023	0.664	0.0310	0.106
	1.450	0.851	0.700	0.0258	0.142
	1.500	0.756	0.711	0.0229	0.153
	1.575	0.616	0.700	0.0187	0.142
	1.650	0.504	0.656	0.0153	0.098
	1.725	0.426	0.606	0.0129	0.048
	1.800	0.526	0.494	0.0159	-0.064
1.085	0.925	0.520	0.167	0.0158	-0.391
	1.000	0.726	0.264	0.0220	-0.294
	1.075	1.210	0.411	0.0367	-0.147
	1.150	1.250	0.575	0.0379	0.017
	1.225	1.018	0.706	0.0308	0.148
	1.300	0.775	0.783	0.0235	0.225
	1.375	0.591	0.833	0.0179	0.275
	1.450	0.494	0.844	0.0150	0.286
	1.500	0.427	0.856	0.0129	0.298
	1.575	0.342	0.858	0.0104	0.300
	1.650	0.256	0.822	0.0077	0.264
	1.725	0.224	0.744	0.0068	0.186
	1.800	0.299	0.617	0.0091	0.059
1.185	0.925	0.272	-----	0.0082	-----
	1.000	0.375	-----	0.0114	-----
	1.075	0.612	-----	0.0185	-----
	1.150	0.551	-----	0.0167	-----
	1.225	0.409	-----	0.0124	-----
	1.575	0.146	-----	0.0044	-----
	1.650	0.115	-----	0.0035	-----
	1.725	0.079	-----	0.0024	-----
	1.800	0.116	-----	0.0035	-----

Table 1 (continued)

$2h/\lambda$	$k_1 b$	V^{sc}/V_r		E^{sc}/E_0	
		Magnitude	Phase (π)	Magnitude	Phase (π)
1.285	0.925	0.063	-----	0.0019	-----
	1.075	0.140	-----	0.0042	-----
	1.150	0.127	-----	0.0038	-----
1.485	0.925	0.124	-----	0.0037	-----
	1.000	0.186	-----	0.0056	-----
	1.075	0.190	-----	0.0058	-----
	1.150	0.175	-----	0.0053	-----
1.585	0.925	0.295	-0.688	0.0089	-1.246
	1.000	0.404	-0.577	0.0122	-1.135
	1.075	0.436	-0.416	0.0132	-0.974
	1.150	0.414	-0.321	0.0125	-0.879
	1.225	0.394	-0.266	0.0119	-0.824
	1.650	0.194	-0.277	0.0059	-0.835
	1.725	0.226	-0.350	0.0068	-0.907
	1.800	0.333	-0.432	0.0101	-0.990
1.785	0.925	0.546	-0.500	0.0165	-1.058
	1.000	0.888	-0.400	0.0269	-0.958
	1.075	1.021	-0.260	0.0309	-0.818
	1.150	1.038	-0.143	0.0314	-0.701
	1.225	1.040	-0.054	0.0315	-0.612
	1.300	1.003	0.001	0.0304	-0.557
	1.375	0.908	0.040	0.0275	-0.518
	1.450	0.801	0.068	0.0243	-0.490
	1.500	0.734	0.068	0.0222	-0.490
	1.575	0.648	0.054	0.0196	-0.504
	1.650	0.550	0.023	0.0166	-0.535
	1.725	0.552	-0.049	0.0167	-0.607
	1.800	0.729	-0.166	0.0221	-0.724
1.985	0.925	0.861	-0.274	0.0261	-0.832
	1.000	1.189	-0.113	0.0360	-0.671
	1.075	1.523	-0.021	0.0461	-0.579
	1.150	1.609	0.112	0.0487	-0.446
	1.225	1.608	0.207	0.0487	-0.351
	1.300	1.508	0.218	0.0457	-0.340
	1.375	1.318	0.312	0.0399	-0.246
	1.450	1.134	0.340	0.0344	-0.218
	1.500	1.045	0.340	0.0317	-0.218
	1.575	0.887	0.343	0.0269	-0.215
	1.650	0.756	0.323	0.0229	-0.235
	1.725	0.695	0.262	0.0210	-0.296
	1.800	0.885	0.123	0.0268	-0.435

Table 1 (continued)

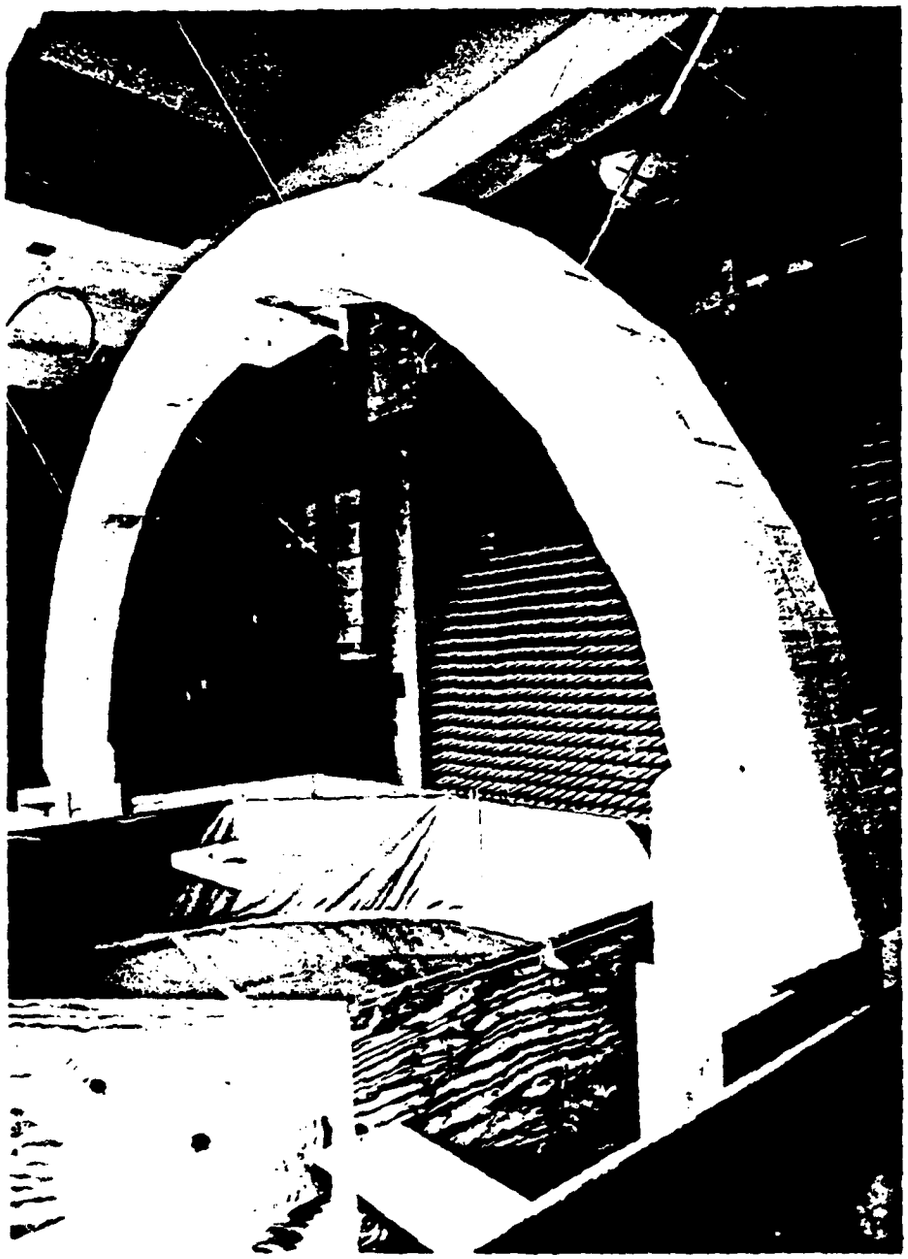

Figure 1 The Experimental Setup

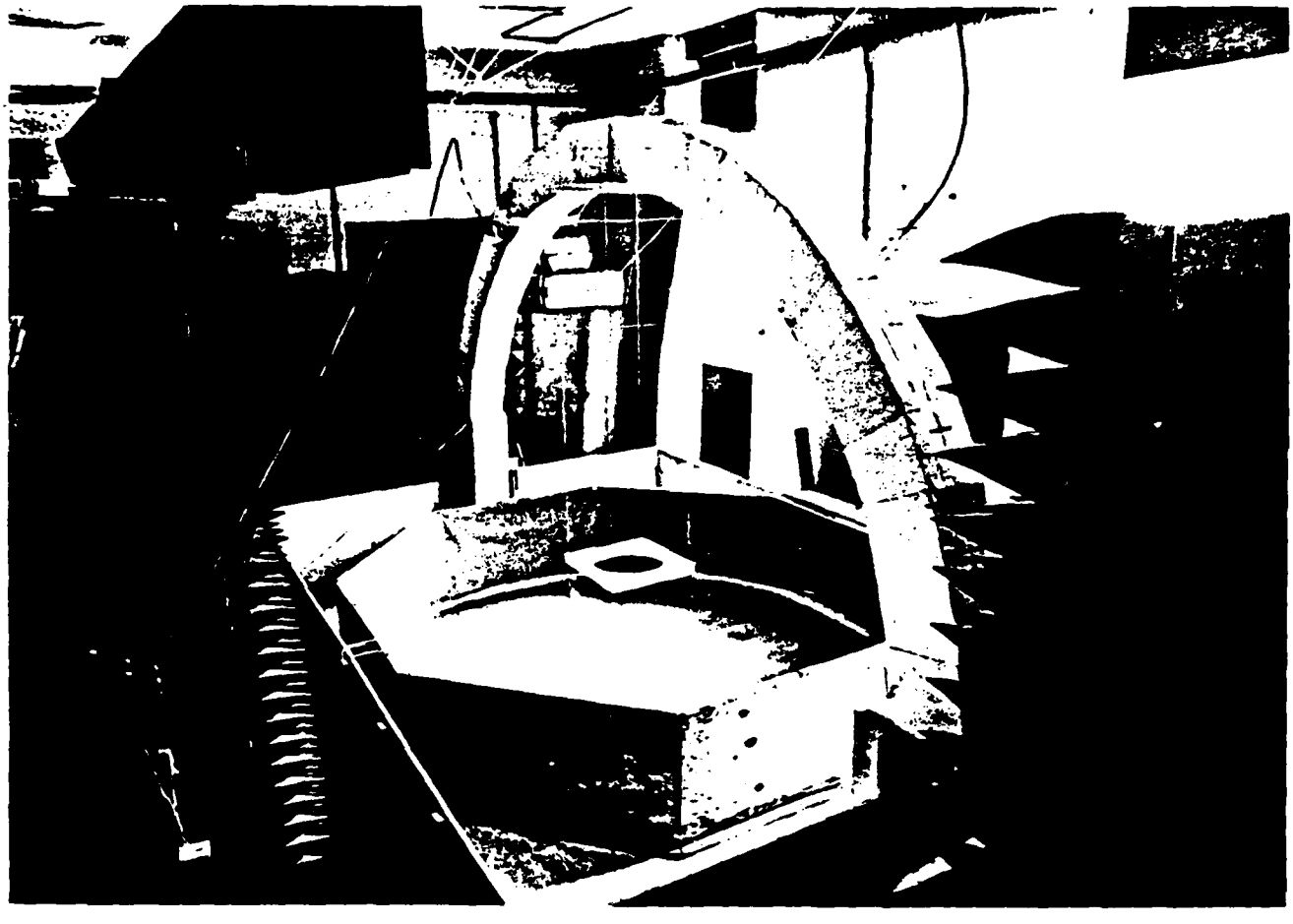

Figure 2 The Experimental Setup, a Different View

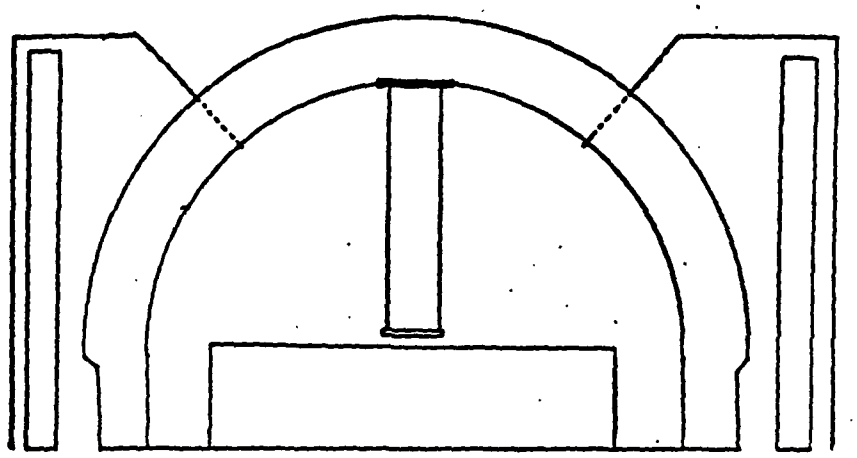

Fig. 3 Schematic Diagram of Mechanical Setup

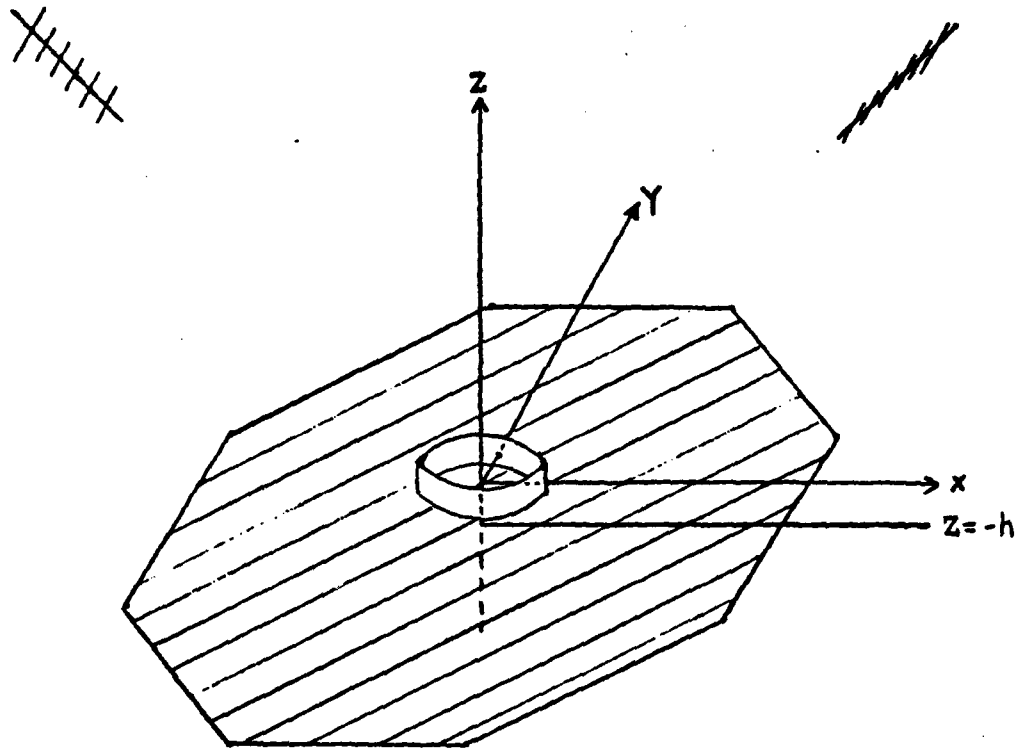

Fig. 4 Diagram of the Mechanical Setup with Styrofoam and Absorbers removed

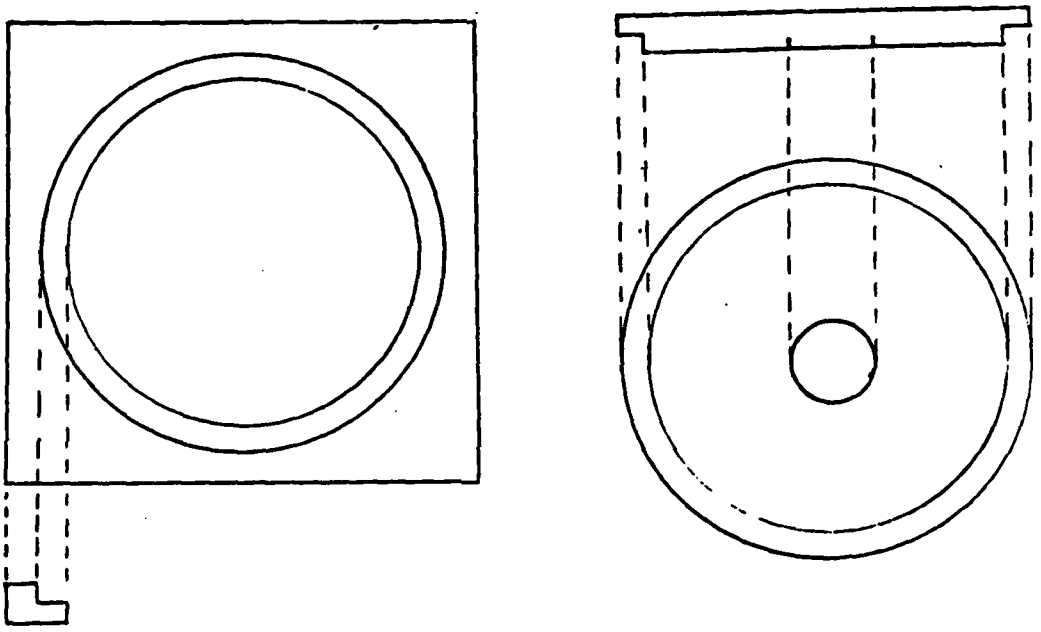

Fig. 5 Styrofoam Disc with an Embedded Fat Tubular Cylinder (right) and Styrofoam Disc Holder (left)

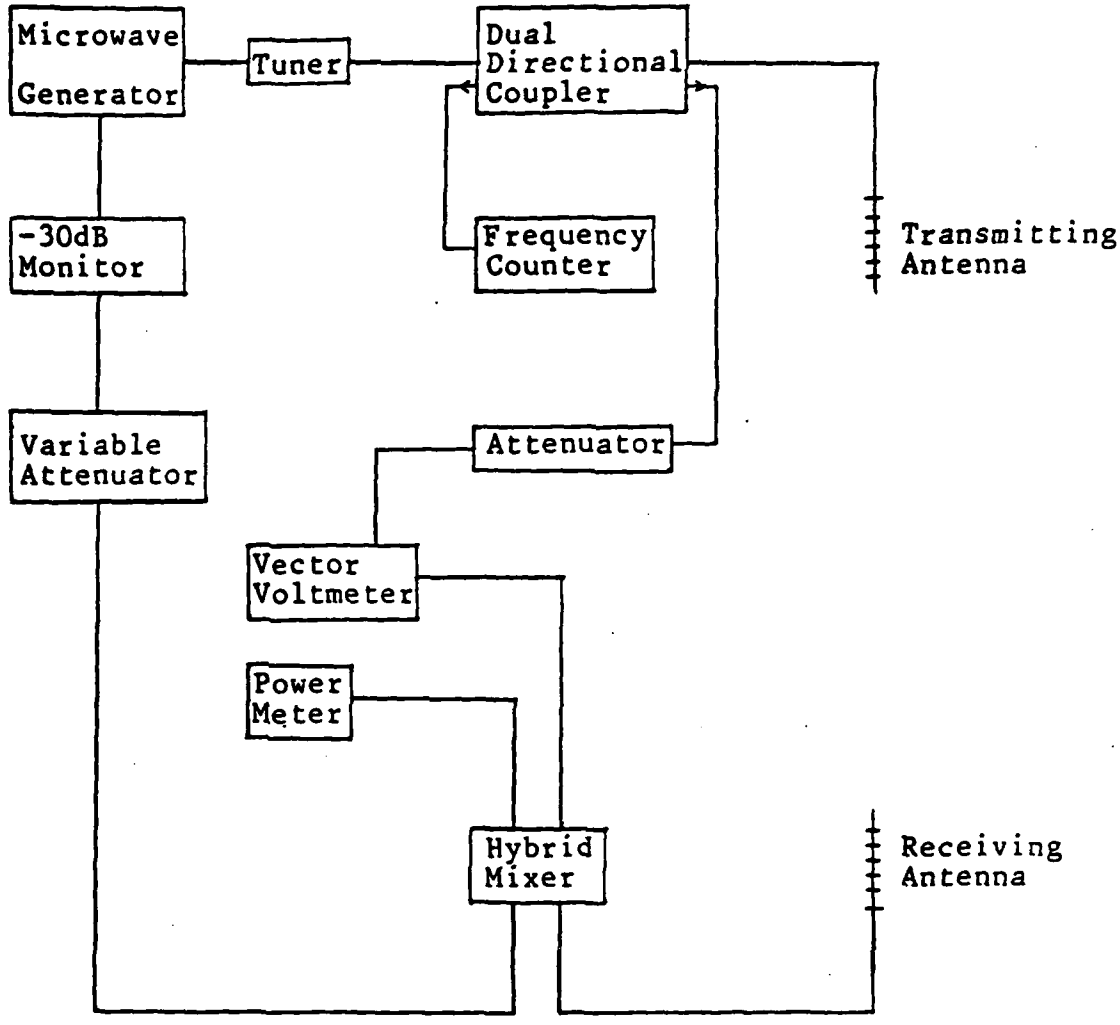

Fig. 6 Block Diagram for the Measuring and Cancellation Circuit

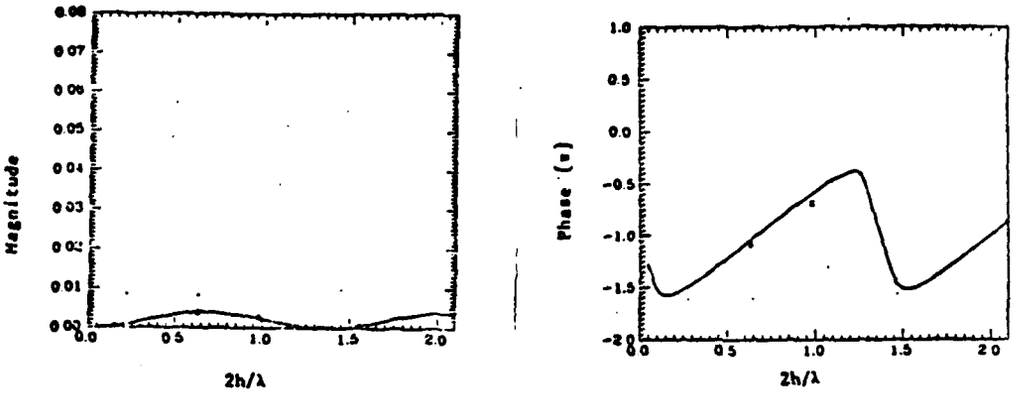

Fig. 7 $k_1 b=0.550$

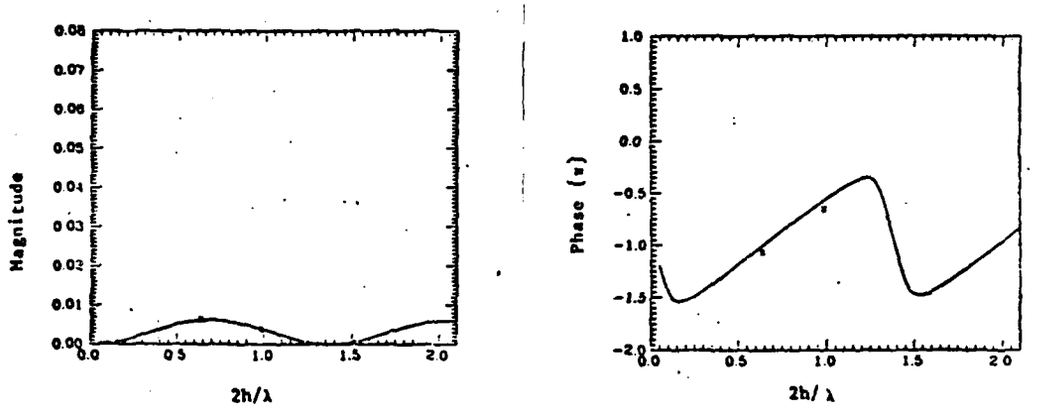

Fig. 8 $k_1 b=0.625$

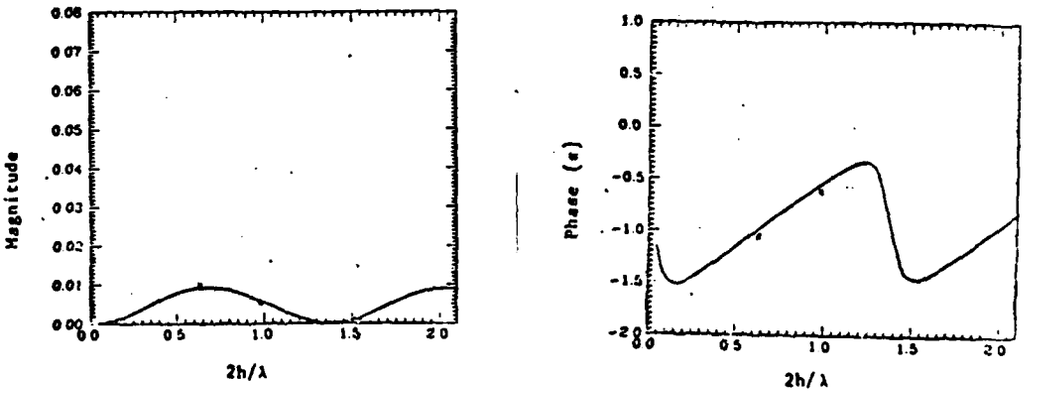

Fig. 9 $k_1 b=0.700$

E^{SC}/E_0 Theory (Solid Lines) and Experiment (X)

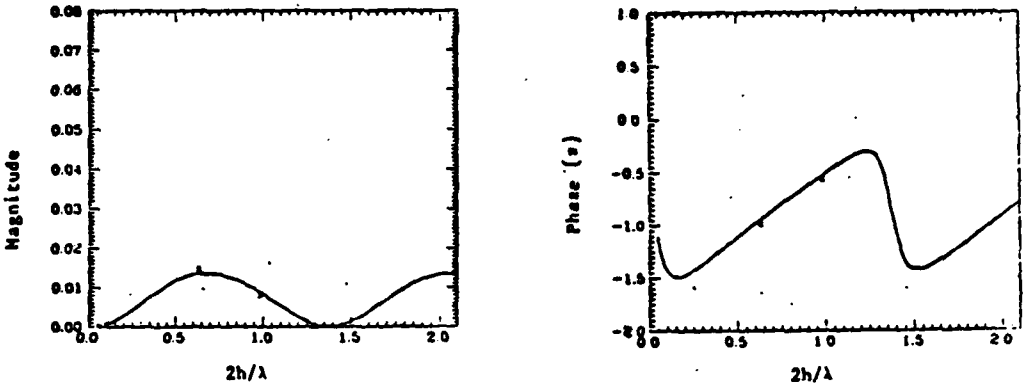

Fig. 10 $k_1 b=0.775$

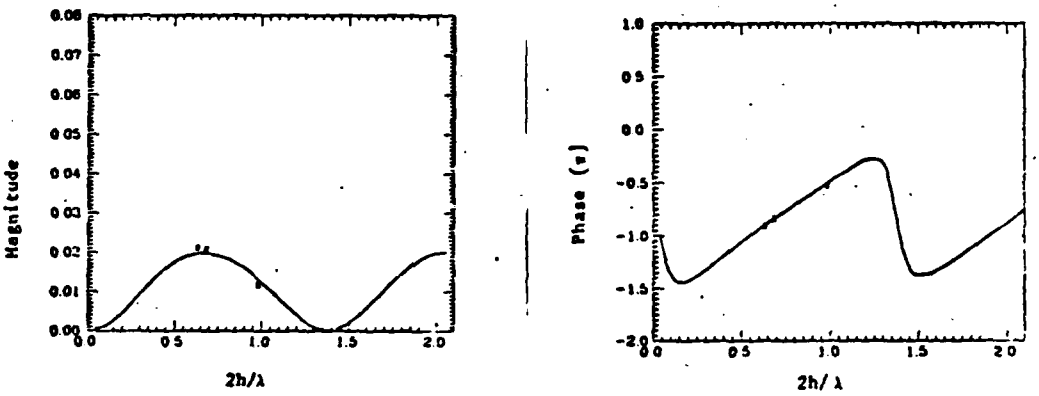

Fig. 11 $k_1 b=0.850$

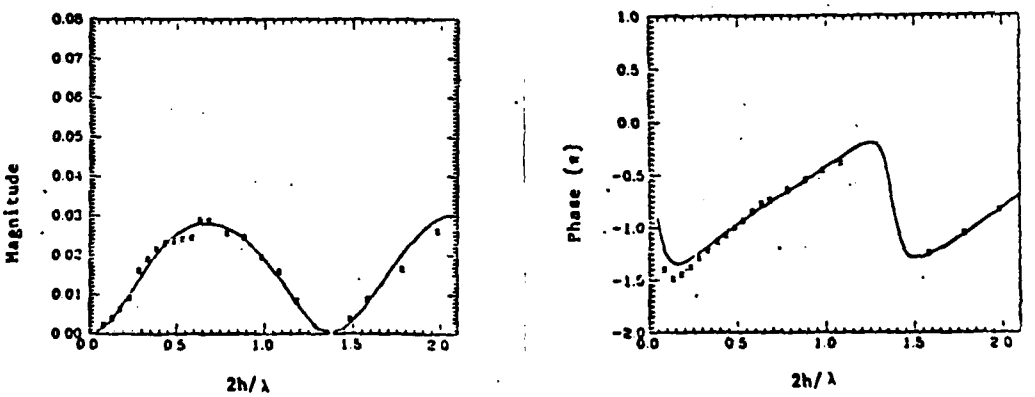

Fig. 12 $k_1 b=0.925$

E^{SC}/E_0 Theory (Solid Lines) and Experiment (X)

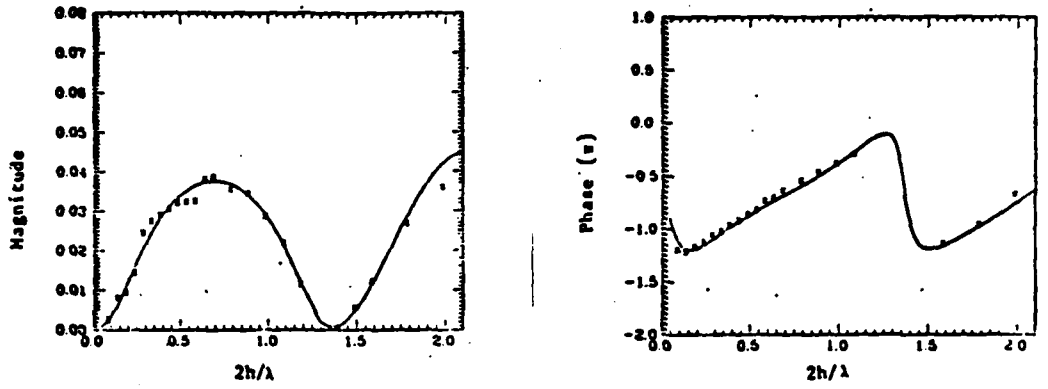

Fig. 13 $k_1 b = 1.000$

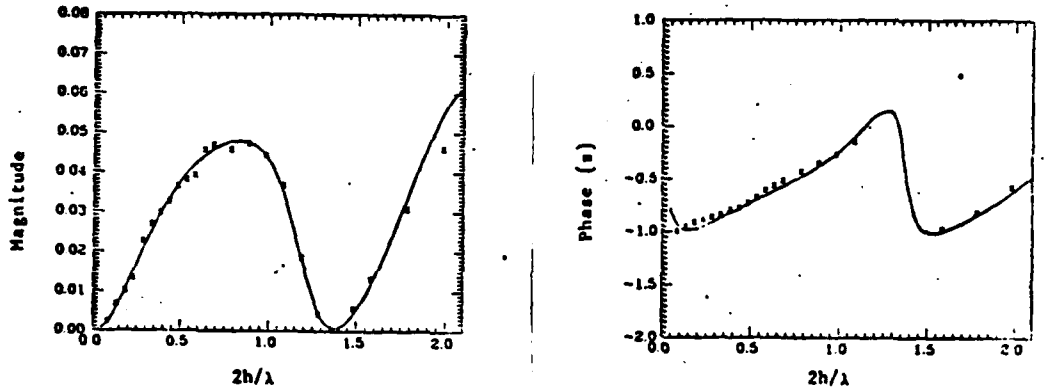

Fig. 14 $k_1 b = 1.075$

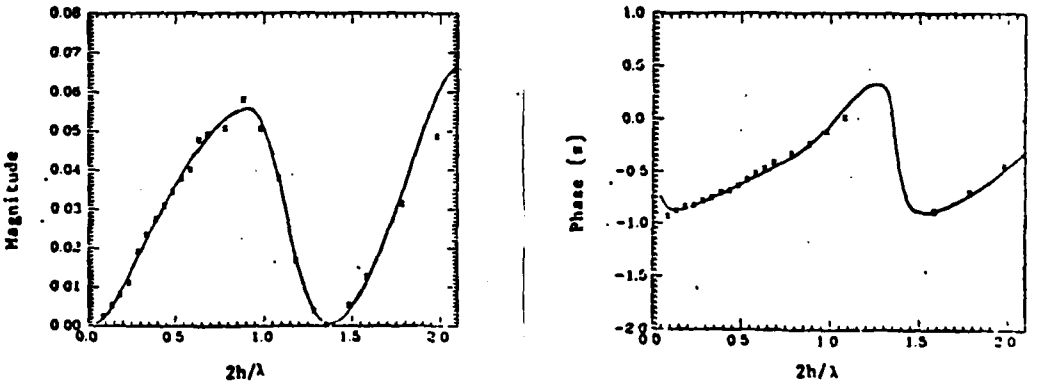

Fig. 15 $k_1 b = 1.150$

E^{SC}/E_0 Theory (Solid Lines) and Experiment (X)

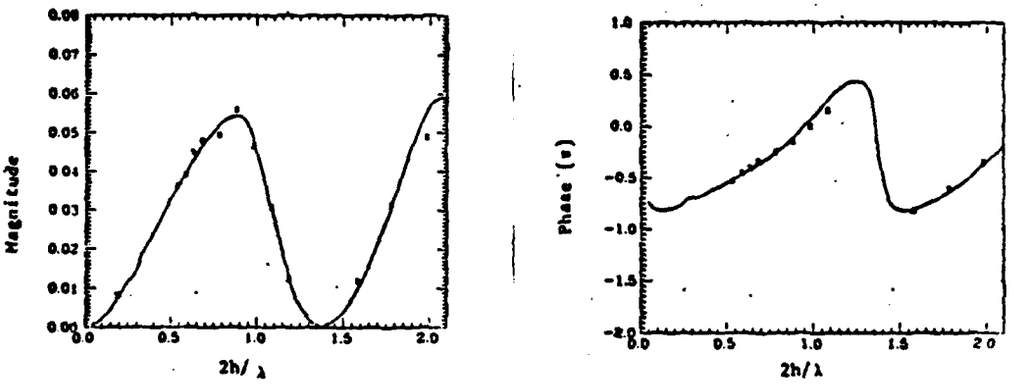

Fig. 16 $k_1 b = 1.225$

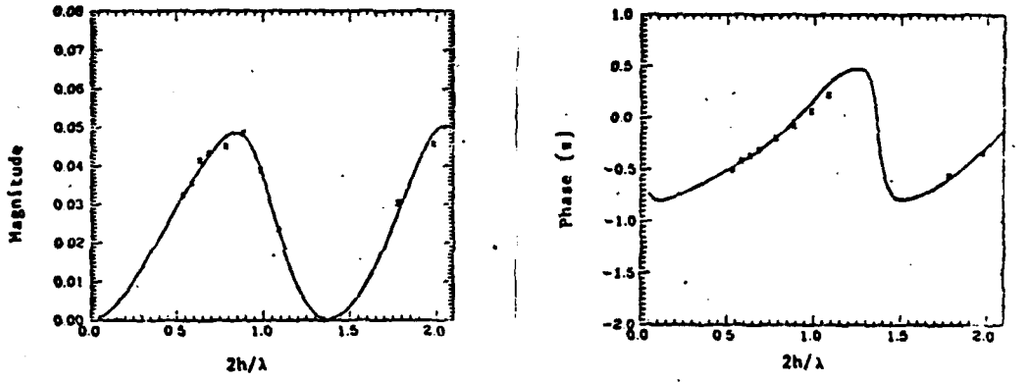

Fig. 17 $k_1 b = 1.300$

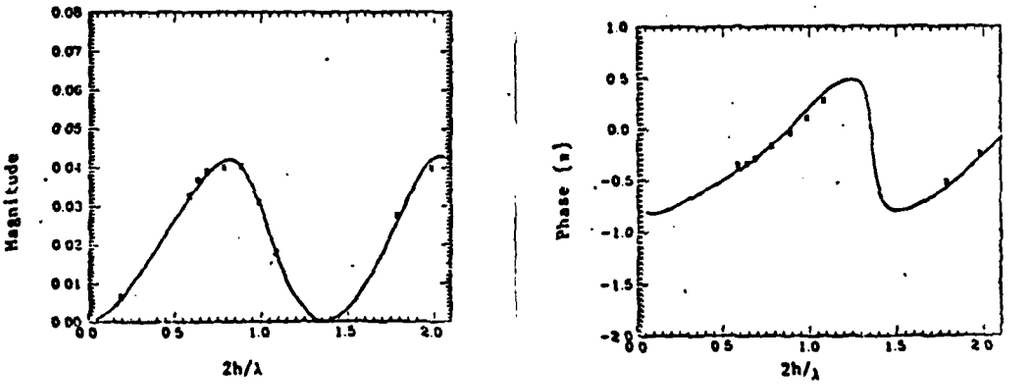

Fig. 18 $k_1 b = 1.375$

E^{SC}/E_0 Theory (Solid Lines) and Experiment (X)

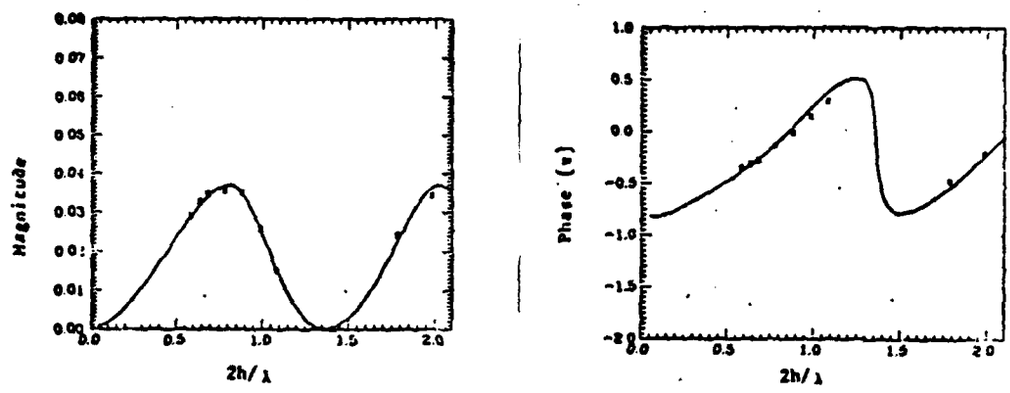

Fig. 19 $k_1 b = 1.450$

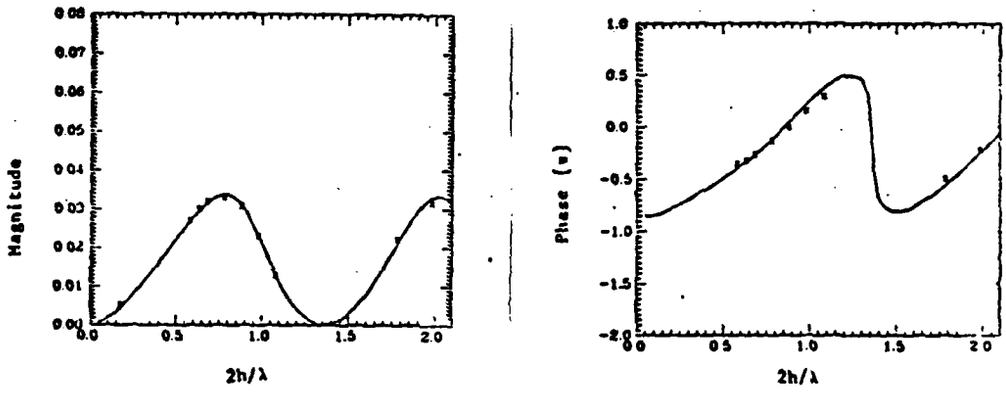

Fig. 20 $k_1 b = 1.500$

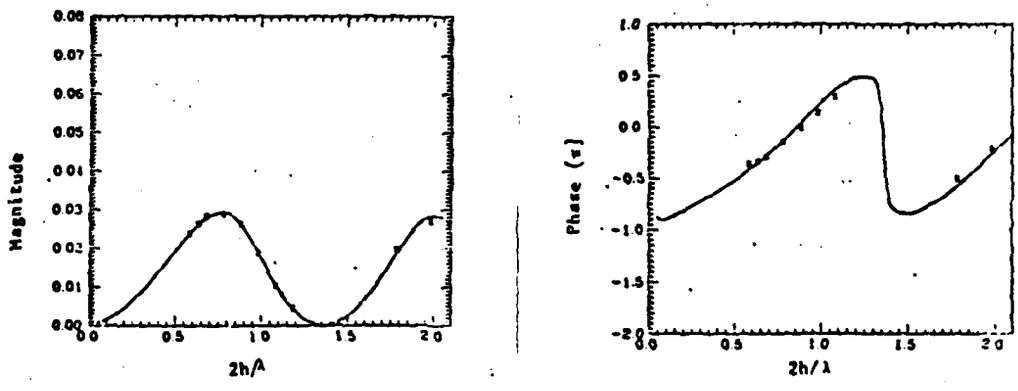

Fig. 21 $k_1 b = 1.575$

E^{SC}/E_0 Theory (Solid Lines) and Experiment (X)

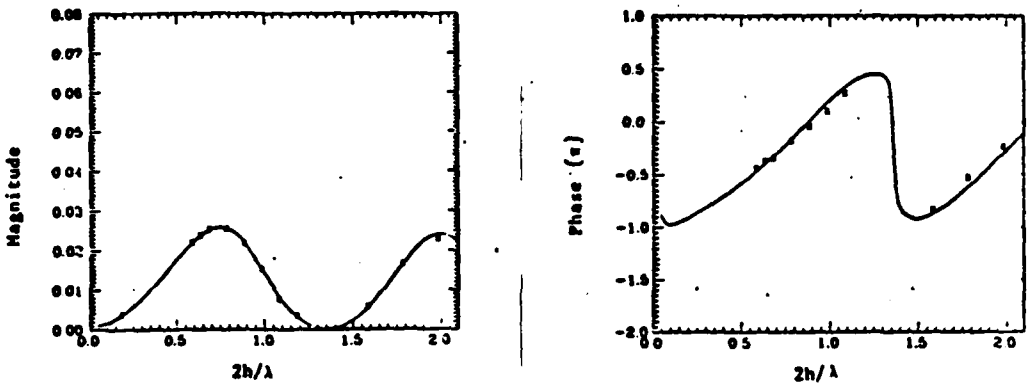

Fig. 22 $k_1 b = 1.650$

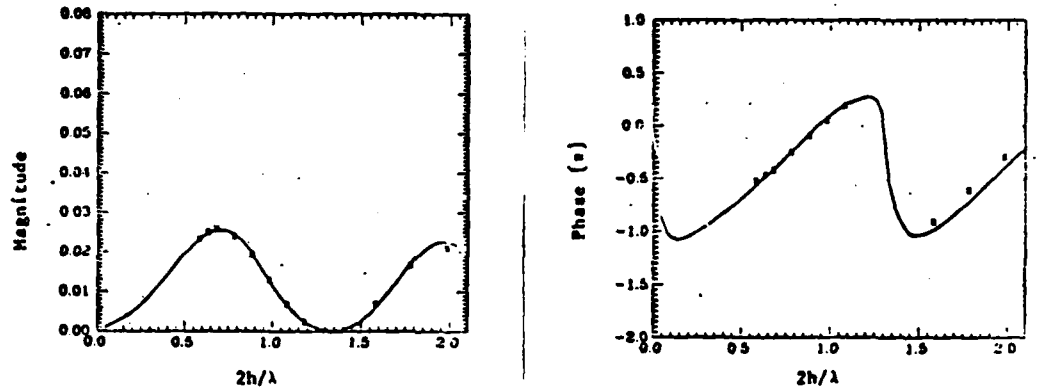

Fig. 23 $k_1 b = 1.725$

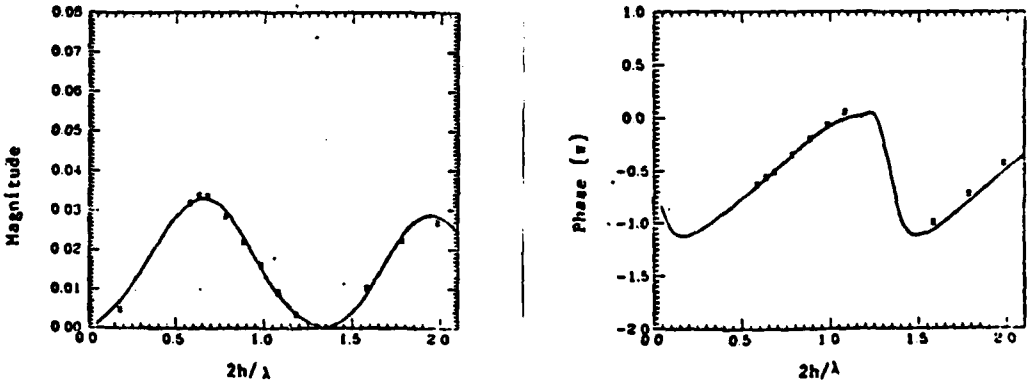

Fig. 24 $k_1 b = 1.800$

E^{SC}/E_0 Theory (Solid Lines) and Experiment (X)

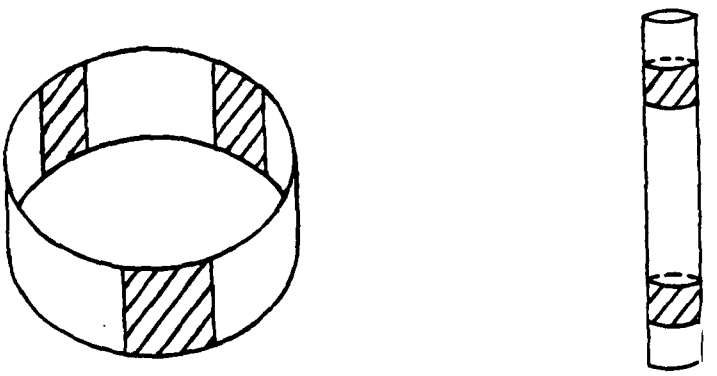

Fig. 25 Patches on Tubular Cylinders
Fat (left) and Thin (right)

LIST OF PUBLICATIONS

1. R. W. P. King and B. H. Sandler, "Analysis of the currents induced in a general cross by a plane wave incident at an angle with arbitrary polarization," IEEE Trans. Antennas Propagation, vol. AP-29, pp. 512-520, May 1981.

2. R. W. P. King, "Currents induced in a wire cross by a plane wave," presented at the 1980 IEEE/AP-S International Symposium held in Quebec, Canada, June 2-6, 1980.

LIST OF PARTICIPATING SCIENTIFIC PERSONNEL

Tai Tsun Wu, Principal Investigator
Ronold W. P. King, Senior Scientist
Liang C. Shen, Senior Scientist
Hung-Mou Lee, Graduate Student*
Margaret Owens, Staff Assistant
Barbara H. Sandler, Mathematician & Programmer

*Mr. H. M. Lee received the Ph.D. degree during the summer of 1981 for work he performed in conjunction with this research project. His thesis is entitled "Electromagnetic Scattering of a Loop Above a Half-Space: Theory and Experiment," Ph.D. Thesis, Harvard University, Cambridge, MA, 1981.

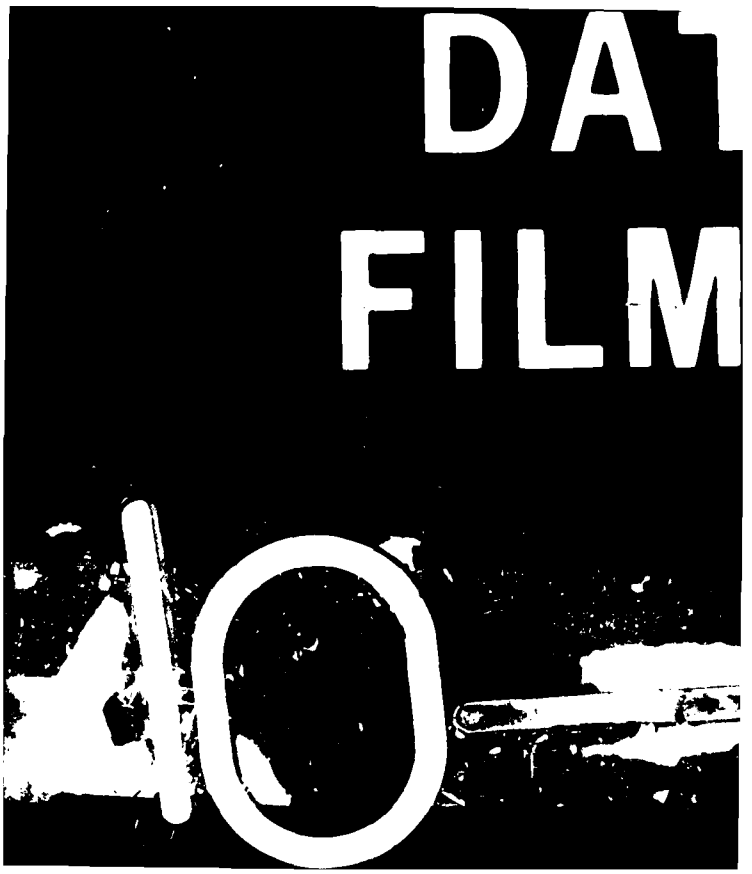
DA
FILM
40